Applied Materials Today 20 (2020) 100712

Contents lists available at ScienceDirect

Applied Materials Today

journal homepage: www.elsevier.com/locate/apmt

Thin-walled Ni-Ti tubes under compression: ideal candidates for efficient and fatigue-resistant elastocaloric cooling

Luka Porenta[a], Parham Kabirifar[a], Andrej Žerovnik[a], Matjaž Čebron[a], Borut Žužek[b], Matej Dolenec[c], Miha Brojan[a], Jaka Tušek[a,*]

[a] Faculty of Mechanical Engineering, University of Ljubljana, Aškerčeva 6, 1000 Ljubljana, Slovenia
[b] Institute of Metals and Technology, Lepi Pot 11, 1000 Ljubljana, Slovenia
[c] Faculty of Natural Sciences and Engineering, University of Ljubljana, Aškerčeva 12, 1000 Ljubljana, Slovenia

ARTICLE INFO

Article history:
Received 17 March 2020
Revised 10 May 2020
Accepted 25 May 2020

Keywords:
Elastocaloric effect
Shape memory alloys
Fatigue life
Compressive loading
Buckling

ABSTRACT

Elastocaloric cooling is emerging as one of the most promising alternatives to vapor-compression cooling technology. It is based on the elastocaloric effect (eCE) of shape memory alloys (SMAs), which occurs due to a stress-induced martensitic transformation (superelasticity). In recent years, several elastocaloric proof-of-concept devices have been developed and the best of them have already achieved commercially relevant cooling characteristics. However, the proposed devices are not yet ready for commercialization, mostly due to their short fatigue life, which is a consequence of the tensile loading. The fatigue life can be significantly improved if the material is instead subjected to compressive loading, but mechanical instabilities (buckling) and the poor heat transfer of bulky geometries (favorable for compression) are the major challenges to overcome when designing compressed elastocaloric elements. Here, we show for the first time that thin-walled Ni-Ti tubes, which allow for the rapid heat transfer, can withstand more than 10^6 compressive loading cycles without any degradation of the eCE while maintaining high efficiency (coefficient of performance) and adiabatic temperature changes as high as 27 K. This is the largest, directly measured, durable eCE for any elastocaloric material in the high-cycle fatigue regime to date, and so opens up new avenues in the development of durable and efficient elastocaloric devices.

1. Introduction

Shape memory alloys (SMAs) have two unique properties, i.e., their shape memory effect and their superelasticity, both of which are consequences of a first-order martensitic transformation between a high-temperature, high-symmetry phase (austenite) and a low-temperature, low-symmetry phase (martensite). An important feature of SMAs that has made them very promising candidates for non-vapor-compression cooling applications [1] is their elastocaloric effect (eCE) [2], i.e., the ability to generate/absorb heat when subjected to a suitable mechanical load. Accordingly, in elastocaloric cooling, superelastic SMAs are mechanically actuated so that the latent heat of the transformation is released to a heat sink (during the forward martensitic transformation) and absorbed by a heat source (during the reverse martensitic transformation). When these transformations occur at high strain rates (i.e., in nearly adiabatic conditions), the latent heat does not have enough time to be transferred to the surroundings and consequently the SMA heats up during loading (forward transformation) and cools down during unloading (reverse transformation). In recent years the elastocaloric behavior of several SMAs has been investigated. The most widely studied elastocaloric alloy is the binary Ni-Ti alloy, in which adiabatic temperature changes of up to approximately 25 K have been measured [3–5]. It has been shown that alloying Ni-Ti with Cu, Co and/or V can reduce the hysteresis [6–8] and increase the fatigue life [9,10], but in turn can reduce the adiabatic temperature changes. The eCE has also been analyzed in some Cu-based [11–13] and Fe-based [14,15] SMAs as well as in magnetic SMAs [16,17] and shape memory polymers [18]. Very recently, a colossal eCE with an adiabatic temperature change of 31.5 K has been discovered in the Ni-Mn-Ti-B alloy system [19]. This is the largest reproducible caloric effect ever measured directly in any solid material. Nevertheless, the structural and functional fatigue behavior of this material has not been studied yet. Furthermore, recent investigations show that additively manufactured Ni-Ti components have

* Corresponding author.
E-mail address: jaka.tusek@fs.uni-lj.si (J. Tušek).

https://doi.org/10.1016/j.apmt.2020.100712

very promising mechanical and elastocaloric properties [20,21], but further research in this relatively new field [22] is necessary before such components can be widely applied. The interesting concept of a composite element (made of a thin Ni-Ti strip and a base polymer) subjected to bending, which can reduce the required forces for the transformation, while keeping the Ni-Ti strips under pure tension or compression loading, has been proposed in [23]. A more comprehensive review of elastocaloric materials can be found in [24,25].

Based on these large and potentially very efficient eCEs, the US Department of Energy [1] and more recently also the European Commission [26] selected elastocaloric cooling as the most promising future alternative to vapor-compression cooling technology, which is over a century old, relatively inefficient and continues to use refrigerants that are harmful to the environment [27]. Due to the expected exponential worldwide increase in cooling and in particular air-conditioning demands in the coming decades [28], the development of an alternative, non-vapor-compression technology is becoming one of the most urgent environmental concerns. Here, elastocaloric cooling can play an important role, since it can be more efficient than vapor-compression [2] and environmentally friendly due to its use of harmless, solid-state refrigerants.

In recent years the first elastocaloric proof-of-concept devices have been developed and tested. They range from single-stage devices with a contact solid-to-solid [29–31] or convective [32] heat transfer to more complex multi-stage devices utilizing heat recovery [33], active regeneration [2,34,35] and cascade [36–38] principles, most of which (except [33,36]) are based on tensile loading. In a single-stage elastocaloric cycle, the maximum temperature span is limited by the adiabatic temperature changes of the elastocaloric material. Therefore, such systems can only operate around the surrounding temperature, without generating a significant temperature span. On the other hand, multi-stage cycles can generate temperature spans that can be much larger than the adiabatic temperature changes of the elastocaloric material itself. This is crucial for most practical cooling applications where temperature spans (between the heat sink and the heat source) of more than 30 K are typically required. To date, the best overall cooling and heat-pumping characteristics have been obtained using active elastocaloric regenerators (analogous to the active magnetic regenerators widely applied in magnetic refrigeration [39]) in which a temperature span of 20 K, a specific heating power of 800 W per kilogram of the elastocaloric material and an exergy efficiency of 20 % were demonstrated [34,35]. The aforementioned elastocaloric regenerator [34] was made out of 0.25 mm thick Ni-Ti dog-bone-shaped sheets that were subjected to tensile loading. In such a geometry, thin walls, a small hydraulic diameter and a large specific heat-transfer area provide fast and efficient heat transfer between the elastocaloric material and the heat-transfer fluid, which results in good cooling and heat-pumping properties, but a very limited fatigue life (only up to 6000 cycles [35]) as a result of the tensile loading.

However, despite the considerable number of studies on the fatigue life of SMAs (mostly the binary Ni-Ti alloy) subjected to tension or bending [40], their fatigue life in compression has been studied much less. For example, it has been shown that in tension, a durable operation (with a high-cycle fatigue of over 10^5 cycles) can be achieved in the Ni-Ti alloy with strains below 2 %, which correspond to relatively small eCEs (up to 8 K) [40,41]. Chluba et al. [9,10] demonstrated an ultra-low-fatigue Ni-Ti-Cu-Co thin film produced by sputtering deposition that can withstand 10 million loading cycles under tension with a strain of up to 2.5 % (and adiabatic temperature changes of up to 10 K). However, the applied sputtering-deposition technique is still too time consuming for the large-scale production of this material, which would be required in practical cooling or heating applications. On the other hand, it has been shown recently that SMAs under compression can have a significantly longer fatigue life compared to those under tension [42,43]. The first studies on Ni-Ti cylinders and cubes under compression confirmed a significant improvement in the fatigue life compared to tension, with up to 70 million loading cycles [44,45]. This is very encouraging, but bulky cylinders or cubes are not particularly interesting for elastocaloric technology (in comparison with thin-walled geometries) because of their poor heat-transfer properties (i.e., the long thermal time constant) and the required high transformation forces due to their large cross-sectional areas. Due to the importance of a rapid heat transfer between the elastocaloric material and the heat-transfer fluid, thin-walled Ni-Ti superelastic tubes loaded in compression appear to be ideal candidates for applications in elastocaloric regenerators. However, prior to their use in elastocaloric regenerators, their buckling stability [46–48], fatigue life and any possible degradation of the elastocaloric effect and its efficiency after fatigue cycling should be investigated in detail, which is the main objective of this work.

In addition, this work presents the new concept of a tube-based structure that can act as an efficient elastocaloric regenerator (Figure 1). Our initial, experimental, thermo-hydraulic evaluation of such a structure shows that it could be an excellent compromise between packed-bed and parallel-plate geometries, which are normally used for solid-state caloric cooling, since they exhibit a high heat-transfer coefficient and a small pressure drop [49]. The seminal idea for this structure was first proposed in 2018 by Tušek et al. [50]. In the structure the tubes are stacked and supported by additional elements that prevent them from buckling and guide the heat-transfer fluid in a cross-flow around each tube (similar to a shell-and-tube heat exchanger). Thus, the fluid flows from the side of the regenerator and not through the bulky and complex loading grips at the top/bottom of the regenerator, as in the case of the first presented tube-based elastocaloric structure [33], where a tight bundle of tubes that support each other is used (and the fluid flows inside the tubes). In the proposed configuration shown in Figure 1, the tubes are completely independent of each other. Therefore, a thorough understanding of a single tube's behavior from the functional and fatigue-life points of view is crucial for the fabrication of the mechanically stable and durable elastocaloric regenerators proposed here. Furthermore, an important feature of the tube-based elastocaloric regenerator shown in Figure 1 is also the possibility of stacking tubes with different properties (i.e., different austenitic transformation finish temperatures – A_f) along the length of the regenerator where the temperature span is established (i.e., a layered elastocaloric regenerator – see [51] for details). Each bundle of tubes in a layered tube-based elastocaloric regenerator (where each covers a portion of the total temperature span) could be made of different tubes with an appropriate A_f that is relatively near their working temperature. With that the temperature range that each tube needs to cover would be smaller and the required transformation stress would be reduced compared to the case where tubes of a single A_f are used along the length of the regenerator. This would also improve the tube's buckling stability as well as the functional stability and adiabatic temperature changes, which, in the case of Ni-Ti alloy, decrease with increasing the temperature range (and consequently the required transformation stress), as shown and discussed in [4, 52]. Applying a layered elastocaloric regenerator, therefore, reduces the otherwise crucial importance of covering a large temperature range with a single elastocaloric element in practical devices (therefore, in this work the tubes are evaluated only at a constant (ambient) temperature, with A_f being –7.3°C). Nevertheless, each elastocaloric material needs to be evaluated at the required temperature range before being employed in an actual device (according to the desired working temperatures and the temperature span). For details on

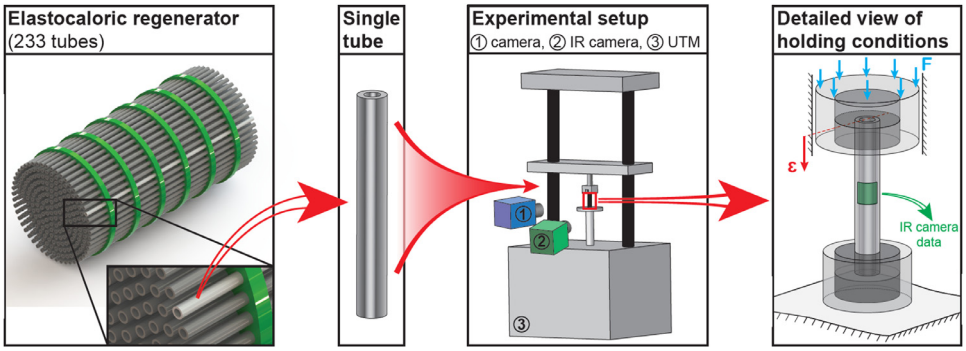

Figure 1. Schematic representation of a tube-based regenerator and the experimental setup for testing a single tube.

the testing of different elastocaloric materials over a wider temperature range see, e.g., [4,8,11,13,15,17].

2. Results and discussion

2.1. Buckling-stability analysis

In the first step of this study the buckling stability of the Ni-Ti thin-walled tubes (with outer diameters of 3 mm and wall thicknesses of 0.25 mm) of various gauge lengths under different compressive loads was investigated both experimentally and theoretically. Figure 1 shows a schematic representation of the experimental setup, which consists of a universal testing machine equipped with an optical and an infrared camera. A special custom-made holder that supports both ends of the tube (see Figure 1) and ensures uniaxial loading of the tubes was used. The details of the buckling-stability experiments are given in Section 4. Materials and methods. Furthermore, a new numerical model for the buckling analysis has been developed to simulate the relationship between the critical buckling stress and the length of the tubes. The model uses 1D truss-beam finite elements based on the Euler-Bernoulli beam theory [53], also including the axial displacement. The details of the model are presented in Appendix A. Supplementary data. Figure 2 (a) shows the critical stresses at which the first instabilities were experimentally detected in tubes of six different lengths and compares them with the model predictions. Both the experimental and simulation results indicate the existence of a critical length below which the buckling stress is high enough to allow for a complete martensitic transformation, i.e., for the material to reach the end of the transformation plateau before the tube buckles. The simulation results are shown for two different boundary conditions, i.e., for simple-simple (SS) and fixed-fixed (FF) supported ends of the tubes. As seen from Figure 2 (a), the model correctly predicts the trend of the dependency, but the critical buckling stresses for tube lengths longer than 12 mm are overpredicted for both boundary conditions. This is most likely due to the 1D nature of the model, which does not account for the local (shell-like) instabilities that initially occur in the tubes (see Figure 2 (b)), and to various existing imperfections in the experiment, e.g., the defects of the geometry of the tubes, the imperfect gripping, etc. On the other hand, the experimentally determined critical length at which the material can be fully transformed without the tube buckling, lies between the results of the two boundary conditions assumed in our model. This indicates that the actual supports at the ends of the tube act elastically (in between the simple and the fixed conditions).

The buckling response is generally a function of the geometry, the material properties and the boundary conditions (type of tube gripping). In uniaxial compressive experiments, such as ours, the tube can act both as a shell (when relatively short) and as a beam (when relatively long). This means that the loss of stability might be localized (a “shell-like” response) and/or that the tube might bend globally (a “beam-like” response). Theoretically, the critical buckling stress of a shell is independent of the length of the shell, whereas the critical buckling stress of a beam scales with the inverse of the square of the beam’s length [54]. In our experiments both types of responses were observed. In the case of a 14 mm long tube (Figure 2 (b)), we find a “shell-like” response with a non-axisymmetric buckling mode with two circumferential waves, i.e., two dimples on the surface of the tube. Therefore, we would expect these tubes to respond as a shell for lengths $\leq$ 14 mm and that the critical buckling stress would not be affected by any further shortening of the tube, but as we find, the tubes are stable at the stress that corresponds to the end of the transformation plateau at lengths $<$ 12 mm. We attribute this response to the boundary effect due to the supported ends of the tube (the conditions near the supports/grips are not the same as in the mid-length of the tube, where it can respond as a shell). This means that if the tube is short enough the dimple wavelength can be comparable or even longer than the length of the unaffected region of the tube, away from the supports, which is why short tubes ($<$ 12 mm) do not buckle at all (even as a shell) and can therefore be loaded over the entire transformation plateau. Furthermore, we find that the tube behaves like a beam when it is relatively long (compared to the diameter), i.e., in the cases of 18 mm and 20 mm, as shown in Figure 2 (c) and (d). Both 18 mm and 20 mm long tubes have a similar snap-buckling mode at the beginning of the phase transformation with an ovalization of the cross-section that is followed by kinking and then by global bending of the whole structure until it collapses. As shown in Figure 2, the 14 mm long tube showed some instability in the first loading cycle, but it only failed in the third cycle, while longer tubes buckled in the first loading cycle. A particularly interesting phenomenon occurred during the testing of 18 mm tubes (Figure 2 (c)), where after the initial instabilities (point 2), the tubes buckled noticeably (point 3) and then unbuckled (point 4) before collapsing (point 5). A similar phenomenon was also observed in another study [55], where it was attributed to a special sequence of softening/stiffening caused by the asymmetrical progress of the phase transformation on the opposite sides of a SMA tube.

2.2. Functional fatigue and fatigue life

In the next step, six identical tubes of 10 mm gauge lengths (safe buckling length) were trained (stabilized) – see Section 4. Materials and methods for details. As shown in Figure 3, during training, the typical stabilization of the superelastic response occurs [4,52,56] where the transformation start stress, hysteresis loop area and recoverable strain decrease in each cycle, while the accumulated residual strain increases. It is interesting to note from

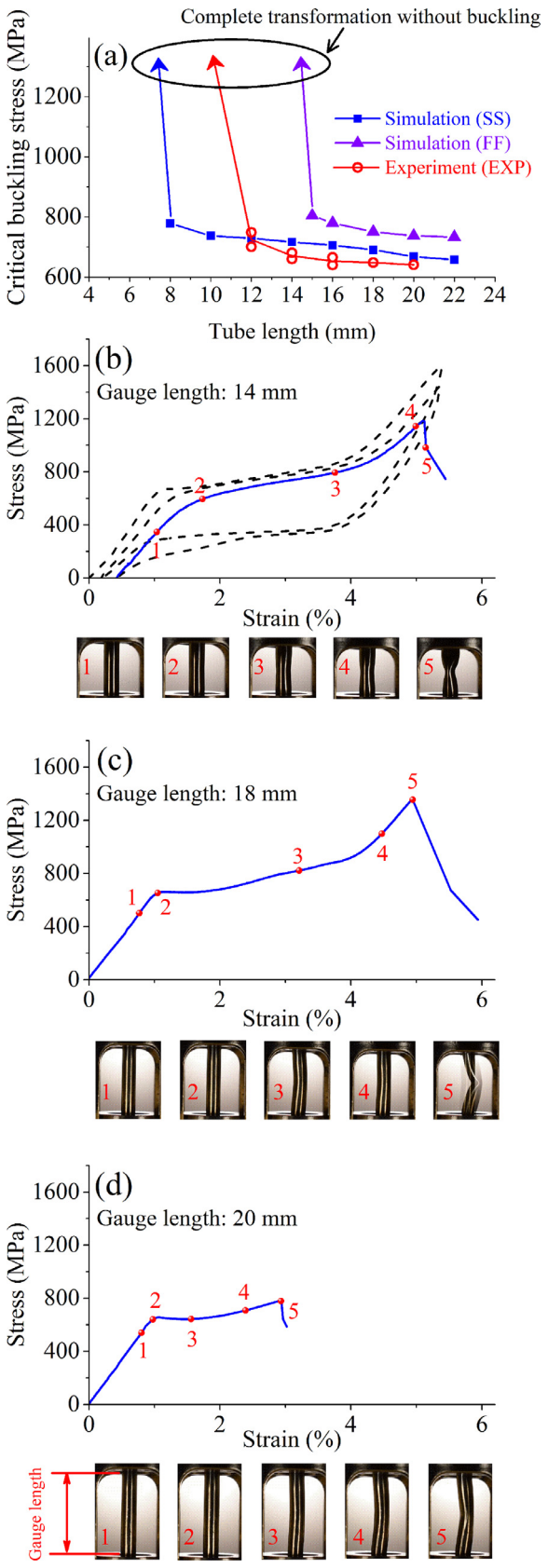

Figure 2. (a) Critical buckling stress of the tubes under compression as a function of a tube's gauge length observed experimentally and predicted by the theoretical model under fixed-fixed (FF) and simple-simple (SS) support conditions and stress-strain curves together with the corresponding images of (b) a tube of 14 mm length, (c) a tube of 18 mm length and (d) a tube of 20 mm length.

Figure 3 that after 100 training cycles the mechanical (superelastic) responses (in particular, the hysteresis loop area and the recoverable strain) are not yet fully stabilized, whereas after only 50 training cycles the temperature changes are already very well stabilized. After the training, four of the six tubes (F1, F2, F3 and F4) were subjected to fatigue cycling, while two tubes (T1 and T2) remained in the trained-only condition to serve as a reference for a later comparison of the adiabatic temperature changes with fatigued tubes (see Section 4. Materials and methods for details). Most importantly, all four fatigue tubes (F1-F4) withstood 10^6 fatigue cycles (set as the runout value) without suffering any visible structural damage, which is one of the most crucial preconditions for practical elastocaloric applications. Figure 4 (a) shows representative stress-strain curves for the fatigue cycling (of tube F3) and Figure 4 (b) shows the variations in the mean hysteresis-loop area and the mean recoverable strain as a function of the number of cycles for all four fatigued tubes (the error bars indicate the standard errors of the mean value). It is evident that although the tubes were trained before the fatigue tests, their mechanical response becomes completely stable only at about 7.0×10^5 cycles (this number is significantly higher compared to the case of tension, where full stabilization was achieved already after 10^4 cycles [41]). To evaluate the functional fatigue from the eCE point of view, the adiabatic temperature changes of all the fatigued tubes (F1-F4) as well as of the trained-only tubes (T1 and T2) were measured. Figure 5 (a) shows the representative adiabatic (for tube F3) and isothermal (for tubes F3 and T1) stress-strain curves. A difference in the isothermal responses of the fatigued and the trained-only tubes, which can be attributed to the additional mechanical stabilization that occurs during fatigue cycling, is clearly visible. Figure 5 (b) shows the mean adiabatic temperature changes as a function of the mean applied strain with their corresponding standard errors of the mean value for the two trained-only tubes and the four fatigued tubes. Both sets of tubes, the trained-only and the fatigued ones, achieved adiabatic temperature changes of 27 K and 20 K at the ends of loading and unloading half cycles, respectively (see Figure 5 (b)). As expected, the adiabatic temperature changes during loading are larger than those of unloading, which is mostly due to the intrinsic mechanical dissipative heat caused by the internal friction in the elastocaloric material during a superelastic cycle that is also manifested through hysteresis [4,5,57]. However, it is very encouraging that the fatigue cycling does not cause any degradation of the thermal response, which is in contrast to the mechanical response under the same conditions (Figure 4 (b)). The adiabatic temperature changes of the fatigued tubes are, especially for the medium applied strains, even noticeably higher than those of the trained-only tubes. This is related to the decrease in the transformation stress during the fatigue cycling, which in turn means that the transformation and the corresponding eCE occur at lower strains (as also noticed in [44]), while the total amount of transformed material remains the same (the adiabatic temperature changes at the end of the transformation plateau are the same for the fatigued and trained-only tubes). To further investigate the impact of the fatigue cycling, an X-ray diffraction analysis on fatigued (F4) and as-received tubes was performed. It is clear from Figure 5 (d) that the residual martensite accumulates because of the fatigue cycling, which is in line with the degradation of the mechanical response (Figure 4). In the fatigued tube (compared to the as-received one) the austenite peaks broaden slightly, their intensity decreases (some peaks are lost in the background and become undetectable) and an additional martensite peak becomes visible, which is in agreement with [58].

Nevertheless, in addition to fast and efficient heat transfer, a precondition for an efficient elastocaloric device is an efficient eCE of the material itself. The efficiency of the elastocaloric material can be expressed through the material's coefficient of performance

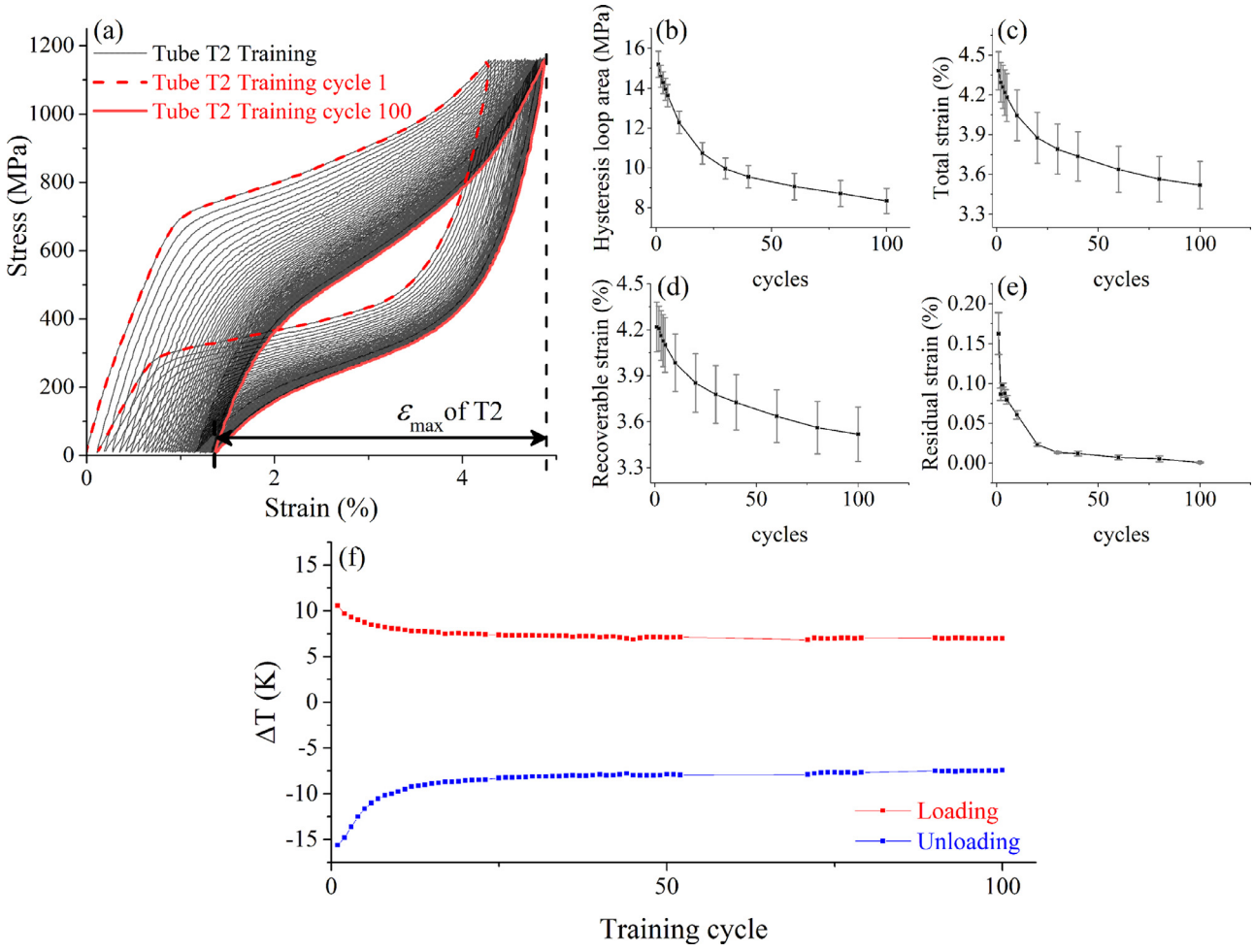

Figure 3. (a) Stress-strain curves of tube T2 during training and variations in (b) the mean hysteresis-loop area, (c) the mean total strain, (d) the mean recoverable strain and (e) the mean residual strain of all the tubes during training (with error bars showing standard errors of the mean values); and (f) temperature changes of tube T2 during loading and unloading as a function of the number of training cycles.

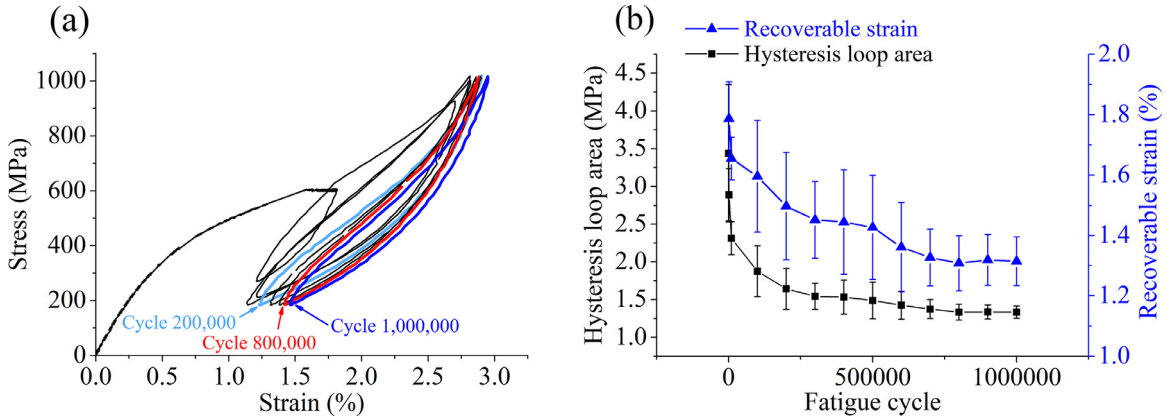

Figure 4. (a) Stress-strain curves of tube F3 during fatigue cycling and (b) the corresponding variations in the mean hysteresis-loop area and the mean recoverable strain as a function of the number of fatigue cycles.

(COP_{mat}) that is defined as the ratio of the heat generated during the elastocaloric effect and the input work required to (un)load the material [59]:

$$COP_{mat} = \frac{\rho \cdot c \cdot \Delta T_{ad}}{\oint \sigma \, d\varepsilon}, \quad (1)$$

where ρ, c, ΔT_{ad}, σ and ε are the density of Ni-Ti (6500 kg/m^3), its specific heat (430 J/kgK), the adiabatic temperature changes, the stress and the strain, respectively. Figure 5 (c) shows the mean material's COP values of the trained-only tubes and the fatigued tubes calculated based on the adiabatic temperature changes (shown in Figure 5 (b)) and the corresponding stress-strain curves (shown in Figure A5 in Appendix A. Supplementary data). We can see that the calculated COP_{mat} values decrease with the applied strain, since the input work increases more rapidly with increasing the strain than the adiabatic temperature changes do. As expected, due to

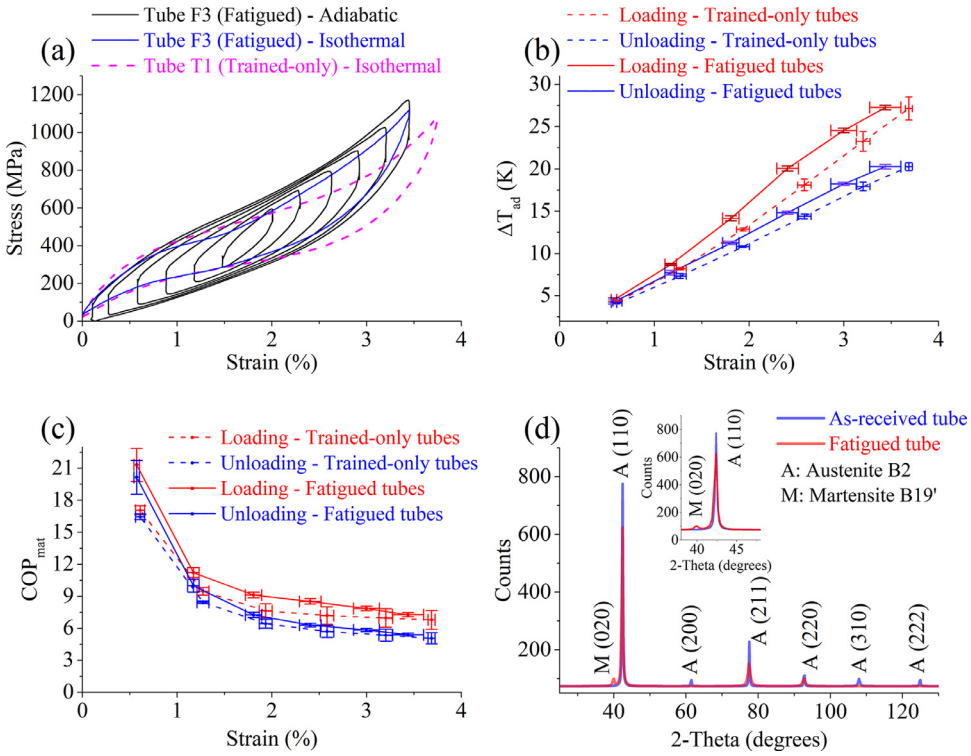

Figure 5. (a) Adiabatic and isothermal stress-strain curves of fatigued tube F3 and isothermal stress-strain curve of trained-only tube T1; (b) mean adiabatic temperature changes (ΔT_{ad}) of the fatigued and the trained-only tubes as a function of mean strain during loading and unloading; (c) mean material's COP values of the trained-only tubes and fatigued tubes as a function of applied strain (error bars indicate standard errors of the mean values) and (d) X-ray diffraction patterns of an as-received and a fatigued tube (F4).

the hysteresis losses, the heating COP_{mat} values (during loading) are larger than the cooling COP_{mat} values (during unloading). As is also clear from Figure 5 (c), the tubes after fatigue cycling exhibit a higher COP_{mat} than the trained-only ones (especially for moderate applied strains), which is mostly due to higher adiabatic temperature changes of the fatigued tubes (see Figure 5 (b)). A maximum COP_{mat} value of above 20 was obtained at the smallest applied strain, while a COP_{mat} of around 6 was obtained at the highest applied strain. These values are, in general, comparable (with respect to the applied strain/stress) with other materials' COP values measured for Ni-Ti cubes, cylinders [44,45] and wires [3] under compressive loading and are higher than those measured under tensile loading [3], thus showing significant potential for developing efficient elastocaloric devices.

3. Conclusions

In summary, we have shown that all the tested thin-walled Ni-Ti superelastic tubes of a safe buckling length can survive more than 10^6 fatigue cycles without any visible structural damage. Subsequent adiabatic cycles applied to both the fatigued and the trained-only tubes showed that in both cases, adiabatic temperature changes of 27 K and 20 K in the loading and unloading half cycles could be generated. This confirms that, in contrast to the mechanical response, the eCE of the tubes does not degrade during the fatigue cycles (and even increases for medium applied strains). The adiabatic temperature changes measured in this study are significantly larger than any other durable adiabatic temperature changes measured to date (considering the studies in which the runout was set for the high-cycle fatigue regime ($\geq 10^5$ cycles)). We have shown that thin-walled elastocaloric tubes (that allow for fast and efficient heat transfer) are very promising geometries for elastocaloric cooling. The fatigue-resistant operation of several identical tubes for over 1 million cycles (in combination with a high, durable and efficient eCE) shows enormous potential for practical applications for which a fatigue life of well over 1 million cycles is commonly required [3]. This should inspire further studies using the combined geometric (buckling stability), material (fatigue) and thermal optimizations of elastocaloric tubes and tube-based elastocaloric regenerators initiated in this work.

4. Materials and methods

4.1. Materials and XRD analysis

Medical grade Ni-Ti tubes of 55.92 wt% Ni, an austenite finish temperature (A_f) of −7.3 °C (determined by Bend and Free Recovery Method in accordance with ASTM F2082 standard), an outer diameter of 3.0 ± 0.01 mm, an inner diameter of 2.5 ± 0.025 mm and different gauge lengths (10 to 20 mm) were supplied by Memry corporation (SAES Group). The outer surfaces of the tubes were centerless ground and the inner surfaces were oxide free. The tubes were produced by a cold-drawing process (according to the manufacturer's standard commercial tubing process), having grains elongated in the longitudinal (drawing) direction with mean sizes of 23.4 ± 1.3 μm (in the longitudinal direction) and 12.5 ± 0.6 μm (in the cross-sectional area). The tubes contain inclusions (TiC) of a mean area of 1.2 ± 0.09 μm^2 and a total area fraction of 1.5 % in the longitudinal direction, while in the cross-sectional area, the inclusions have a mean area of 0.4 ± 0.03 μm^2 and a total area fraction of 0.6 % (which is within the manufacturer's and ASTM F2063 standards).

An X-ray diffraction analysis (XRD) was performed using a Philips PW3710 X-ray diffractometer with Cu-Kα radiation (Kα_1=1.54060 Å), a proportional counter and a secondary graphite monochromator at a voltage of 40 kV and a filament current of

30 mA. A flat surface, which was required for the XRD, was created along the length of the tubes by fine polishing the side of the tubes and a 2θ range of 25° to 130° was scanned (see Figure 5 (d)). Austenite (A) and martensite (M) peaks were indexed according to the standard diffraction cards (PDF) 03-065-0917 and 00-019-0850 (for A) and 00-035-281 (for M). By comparing the presented diffraction patterns (shown in Figure 5(d)) with standard PDF cards, it can be observed that the relative peak intensities are different, and some peaks are absent in the current patterns. Since the tubes were cold drawn, this could be a good indication of the presence of texture. Some other mechanical properties of the tubes under consideration are also presented in Table A1 of Appendix A. Supplementary data.

4.2. Buckling-stability testing and stabilization

The buckling stability was tested at a strain rate of 3×10^{-3} s^{-1} up to a maximum stress of 1600 MPa. The training (stabilization) was performed for 100 loading-unloading cycles at a strain rate of 2.3×10^{-3} s^{-1} between 10 MPa and 1150 MPa. The maximum strain that is completely recovered in the last training cycle of each tube (ε_{max}) was used in subsequent adiabatic and isothermal experiments. A Zwick Z050 universal testing machine (UTM) equipped with an Xforce P load cell, with a measuring range of $\pm$ 5 kN and an accuracy of $\pm$ 0.4 % of full scale (FS), was used for this set of experiments. The deformation of the tubes was measured with a long-stroke Zwick extensometer with an accuracy of $\pm$ 0.002 mm. The tube buckling was monitored with a Nikon D 5600 camera equipped with an AF-P DX 18–55mm f/3.5-5.6G lens. All the tests (including the fatigue and adiabatic/isothermal testing) were performed at ambient temperature (24 $\pm$ 2°C).

4.3. Fatigue testing

In the fatigue testing, the tubes were initially loaded to the middle of the transformation plateau and then cycled in load-controlled conditions between 185 MPa and 1015 MPa (full transformation plateau range) with a cycling frequency of 5 Hz. By applying this stress range, straining of the pure austenitic phase without the transformation (and therefore no eCE) was avoided [41]. The runout was set to 10^6 cycles. For the fatigue experiments, an Instron 8802 servo-hydraulic UTM, equipped with a 25 kN load cell with an uncertainty of $\pm$ 0.50 % FS, was used and the strain was measured with an Instron 2620-604 clip-on extensometer with a measuring range of 15 mm and a measurement error of 0.1 % FS.

4.4. Adiabatic/isothermal testing

Prior to the adiabatic tests, the strain rate that fulfills the adiabatic condition was evaluated. Tube T1 was compressed at a wide range of strain rates (9.1×10^{-5} s^{-1} to 0.1 s^{-1}) between 0.14 % and ε_{max} of tube T1, which was 4.47 %. Based on this, a strain rate of 6.8×10^{-2} s^{-1}, which fulfilled the adiabatic conditions, was applied for further adiabatic experiments. The corresponding stress-strain curves and the temperature changes are shown in Figure A6 of Appendix A. Supplementary data.

Six strain ranges, each consisting of three sequential adiabatic cycles (at 6.8 × 10-2 s^{-1}), were applied to each tube and the stress-strain responses and adiabatic temperature changes were recorded (Figure 5 (a) and (b)). To be consistent with the loading paths of the fatigue cycles, the adiabatic cycles were applied to all the tubes around the middle of the transformation plateau (Figure A5 of Appendix A. Supplementary data). As seen from Figure A7 of Appendix A. Supplementary data, cycling the Ni-Ti tubes around the middle of the transformation plateau in compression does not significantly increase the adiabatic temperature changes compared to no pre-strain conditions (which is in contrast to tension, where due to a flatter transformation plateau the advantage of the pre-strain condition is more pronounced [41]). In all the adiabatic tests, the strains were held constant for 60 s at the end of each loading and unloading half cycle to allow the tube's temperature to reach the ambient temperature before the next loading/unloading step begins. Isothermal cycles were performed at a strain rate of 9.1×10^{-5} s^{-1} between 0.14 % and the ε_{max} of each tube. All the adiabatic and isothermal tests were performed on the same setup (Zwick UTM) that was used for the stabilization and the buckling-stability testing.

The temperature changes were measured in the middle of the tube using a FLIR A6750sc infrared camera with an absolute accuracy of $\pm$ 2 % of the reading, equipped with a lens of 50 mm focal length and a 640 × 512 pixel IR sensor with a spatial resolution of 15 μm. With a noise-equivalent differential temperature (NEDT) of below 20 mK, the measurement uncertainty of the temperature difference between the individual pixels is much smaller than the absolute temperature uncertainty of the camera. To capture the rapid temperature changes at high strain rates, the thermal images were recorded with a frame rate of up to 120 Hz. The samples were coated with a thin layer of LabIR paint for standard applications with an emissivity of 0.92.

Data availability

All data used to generate these results is available in the main text or supplementary materials. Further details could be obtained from the corresponding authors upon request.

Declaration of Competing Interest

The authors declare that they have no known competing financial interests or personal relationships that could have appeared to influence the work reported in this paper.

CRediT authorship contribution statement

Luka Porenta: Software, Investigation, Visualization, Writing - original draft. **Parham Kabirifar:** Investigation, Formal analysis, Visualization, Writing - original draft. **Andrej Žerovnik:** Investigation. **Matjaž Čebron:** Validation, Writing - review & editing. **Borut Žužek:** Resources. **Matej Dolenec:** Resources. **Miha Brojan:** Supervision, Resources, Writing - review & editing. **Jaka Tušek:** Conceptualization, Supervision, Funding acquisition, Writing - review & editing.

Acknowledgements

This work was supported by European Research Council (ERC) under Horizon 2020 research and innovation program (ERC Starting Grant No. 803669).

Supplementary materials

Supplementary material associated with this article can be found, in the online version, at doi:10.1016/j.apmt.2020.100712.

References

[1] Navigant Consulting Inc., Energy Savings Potential and RD&D Opportunities for Non-Vapor-Compression HVAC Technologies, 2014. https://doi.org/10.2172/1220817.

[2] J. Tušek, K. Engelbrecht, R. Millán-Solsona, L. Mañosa, E. Vives, L.P. Mikkelsen, N. Pryds, The Elastocaloric Effect: A Way to Cool Efficiently, Adv. Energy Mater. 5 (2015) 1500361 https://doi.org/10.1002/aenm.201500361.

[3] J. Cui, Y. Wu, J. Muehlbauer, Y. Hwang, R. Radermacher, S. Fackler, M. Wuttig, I. Takeuchi, Demonstration of high efficiency elastocaloric cooling with large Δt using NiTi wires, Appl. Phys. Lett. 101 (2012) 073904 https://doi.org/10.1063/1.4746257.
[4] J. Tušek, K. Engelbrecht, L.P. Mikkelsen, N. Pryds, Elastocaloric effect of Ni-Ti wire for application in a cooling device, J. Appl. Phys. 117 (2015) 124901 https://doi.org/10.1063/1.4913878.
[5] H. Ossmer, F. Lambrecht, M. Gültig, C. Chluba, E. Quandt, M. Kohl, Evolution of temperature profiles in TiNi films for elastocaloric cooling, Acta Mater 81 (2014) 9–20 https://doi.org/10.1016/j.actamat.2014.08.006.
[6] J. Frenzel, A. Wieczorek, I. Opahle, B. Maaß, R. Drautz, G. Eggeler, On the effect of alloy composition on martensite start temperatures and latent heats in Ni–Ti-based shape memory alloys, Acta Mater 90 (2015) 213–231 https://doi.org/10.1016/j.actamat.2015.02.029.
[7] A. Wieczorek, J. Frenzel, M. Schmidt, B. Maaß, S. Seelecke, A. Schütze, G. Eggeler, Optimizing Ni–Ti-based shape memory alloys for ferroic cooling, Funct. Mater. Lett. 10 (2017) 1740001 https://doi.org/10.1142/S179360471740001X.
[8] H. Chen, F. Xiao, X. Liang, Z. Li, Z. Li, X. Jin, T. Fukuda, Giant elastocaloric effect with wide temperature window in an Al-doped nanocrystalline Ti–Ni–Cu shape memory alloy, Acta Mater 177 (2019) 169–177 https://doi.org/10.1016/j.actamat.2019.07.033.
[9] C. Chluba, W. Ge, R. Lima de Miranda, J. Strobel, L. Kienle, E. Quandt, M. Wuttig, Ultralow-fatigue shape memory alloy films, Science 348 (2015) 1004–1007 (80-.) https://doi.org/10.1126/science.1261164 .
[10] C. Chluba, H. Ossmer, C. Zamponi, M. Kohl, E. Quandt, Ultra-Low Fatigue Quaternary TiNi-Based Films for Elastocaloric Cooling, Shape Mem. Superelasticity. 2 (2016) 95–103 https://doi.org/10.1007/s40830-016-0054-3.
[11] L. Mañosa, S. Jarque-Farnos, E. Vives, A. Planes, Large temperature span and giant refrigerant capacity in elastocaloric Cu-Zn-Al shape memory alloys, Appl. Phys. Lett. (2013) 103 https://doi.org/10.1063/1.4832339.
[12] S. Qian, Y. Geng, Y. Wang, T.E. Pillsbury, Y. Hada, Y. Yamaguchi, K. Fujimoto, Y. Hwang, R. Radermacher, J. Cui, Y. Yuki, K. Toyotake, I. Takeuchi, Elastocaloric effect in CuAlZn and CuAlMn shape memory alloys under compression, Philos. Trans. R. Soc. A Math. Phys. Eng. Sci. 374 (2016) 20150309 https://doi.org/10.1098/rsta.2015.0309.
[13] S. Xu, H.-Y. Huang, J. Xie, S. Takekawa, X. Xu, T. Omori, R. Kainuma, Giant elastocaloric effect covering wide temperature range in columnar-grained Cu 71.5 Al 17.5 Mn 11 shape memory alloy, APL Mater. 4 (2016) 106106 https://doi.org/10.1063/1.4964621.
[14] F. Xiao, T. Fukuda, T. Kakeshita, Significant elastocaloric effect in a Fe-31.2Pd (at. %) single crystal, Appl. Phys. Lett. 102 (2013) 161914 https://doi.org/10.1063/1.4803168.
[15] F. Xiao, T. Fukuda, T. Kakeshita, X. Jin, Elastocaloric effect by a weak first-order transformation associated with lattice softening in an Fe-31.2Pd (at.%) alloy, Acta Mater. 87 (2015) 8–14. https://doi.org/10.1016/j.actamat.2015.01.004.
[16] J. Liu, D. Zhao, Y. Li, Exploring Magnetic Elastocaloric Materials for Solid-State Cooling, Shape Mem. Superelasticity. 3 (2017) 192–198 https://doi.org/10.1007/s40830-017-0118-z.
[17] F. Xiao, M. Jin, J. Liu, X. Jin, Elastocaloric effect in Ni 50 Fe 19 Ga 27 Co 4 single crystals, Acta Mater 96 (2015) 292–300 https://doi.org/10.1016/j.actamat.2015.05.054.
[18] Z. Xie, G. Sebald, D. Guyomar, Temperature dependence of the elastocaloric effect in natural rubber, Phys. Lett. A. 381 (2017) 2112–2116 https://doi.org/10.1016/j.physleta.2017.02.014.
[19] D. Cong, W. Xiong, A. Planes, Y. Ren, L. Mañosa, P. Cao, Z. Nie, X. Sun, Z. Yang, X. Hong, Y. Wang, Colossal Elastocaloric Effect in Ferroelastic Ni-Mn-Ti Alloys, Phys. Rev. Lett. 122 (2019) 255703 https://doi.org/10.1103/PhysRevLett.122.255703.
[20] H. Hou, E. Simsek, T. Ma, N.S. Johnson, S. Qian, C. Cissé, D. Stasak, N. Al Hasan, L. Zhou, Y. Hwang, R. Radermacher, V.I. Levitas, M.J. Kramer, M.A. Zaeem, A.P. Stebner, R.T. Ott, J. Cui, I. Takeuchi, Fatigue-resistant high-performance elastocaloric materials made by additive manufacturing, Science (80-.). 366 (2019) 1116–1121 https://doi.org/10.1126/science.aax7616.
[21] Q. Zhang, S. Hao, Y. Liu, Z. Xiong, W. Guo, Y. Yang, Y. Ren, L. Cui, L. Ren, Z. Zhang, The microstructure of a selective laser melting (SLM)-fabricated NiTi shape memory alloy with superior tensile property and shape memory recoverability, Appl. Mater. Today. 19 (2020) 100547 https://doi.org/10.1016/j.apmt.2019.100547.
[22] M. Elahinia, N. Shayesteh Moghaddam, M. Taheri Andani, A. Amerinatanzi, B.A. Bimber, R.F. Hamilton, Fabrication of NiTi through additive manufacturing: A review, Prog. Mater. Sci. 83 (2016) 630–663 https://doi.org/10.1016/j.pmatsci.2016.08.001.
[23] A. Czernuszewicz, L. Griffith, J. Slaughter, V. Pecharsky, Low-force compressive and tensile actuation for elastocaloric heat pumps, Appl. Mater. Today. 19 (2020) 100557 https://doi.org/10.1016/j.apmt.2020.100557.
[24] L. Mañosa, A. Planes, Materials with Giant Mechanocaloric Effects: Cooling by Strength, Adv. Mater. (2017) 29 https://doi.org/10.1002/adma.201603607.
[25] P. Kabirifar, A. Žerovnik, Ž. Ahčin, L. Porenta, M. Brojan, J. Tušek, Elastocaloric Cooling, State-of-the-art and Future Challenges in Designing Regenerative Elastocaloric Devices, Strojniški Vestn. – J. Mech. Eng. 65 (2019) 615–630 https://doi.org/10.5545/sv-jme.2019.6369.
[26] VHK, ARMINES, Technology Roadmap in preparatory/review study on Commission Regulation (EC) No. 643/2009 with regard to ecodesign requirements for household refrigeration appliances and Commission Delegated Regulation (EU) No. 1060/2010 with regard to energy labelling o, 2016. www.ecodesign-fridges.eu.
[27] M.O. McLinden, J.S. Brown, R. Brignoli, A.F. Kazakov, P.A. Domanski, Limited options for low-global-warming-potential refrigerants, Nat. Commun 8 (2017) 14476 https://doi.org/10.1038/ncomms14476.
[28] M. Isaac, D.P. van Vuuren, Modeling global residential sector energy demand for heating and air conditioning in the context of climate change, Energy Policy 37 (2009) 507–521 https://doi.org/10.1016/j.enpol.2008.09.051.
[29] M. Schmidt, A. Schütze, S. Seelecke, Scientific test setup for investigation of shape memory alloy based elastocaloric cooling processes, Int. J. Refrig. 54 (2015) 88–97 https://doi.org/10.1016/j.ijrefrig.2015.03.001.
[30] H. Ossmer, F. Wendler, M. Gueltig, F. Lambrecht, S. Miyazaki, M. Kohl, Energy-efficient miniature-scale heat pumping based on shape memory alloys, Smart Mater. Struct. 25 (2016) 085037 https://doi.org/10.1088/0964-1726/25/8/085037.
[31] F. Bruederlin, L. Bumke, C. Chluba, H. Ossmer, E. Quandt, M. Kohl, Elastocaloric Cooling on the Miniature Scale: A Review on Materials and Device Engineering, Energy Technol 6 (2018) 1588–1604 https://doi.org/10.1002/ente.201800137.
[32] S.-M. Kirsch, F. Welsch, N. Michaelis, M. Schmidt, A. Wieczorek, J. Frenzel, G. Eggeler, A. Schütze, S. Seelecke, NiTi-Based Elastocaloric Cooling on the Macroscale: From Basic Concepts to Realization, Energy Technol 6 (2018) 1567–1587 https://doi.org/10.1002/ente.201800152.
[33] S. Qian, J. Ling, Y. Hwang, R. Radermacher, I. Takeuchi, Thermodynamics cycle analysis and numerical modeling of thermoelastic cooling systems, Int. J. Refrig. 56 (2015) 65–80 https://doi.org/10.1016/j.ijrefrig.2015.04.001.
[34] J. Tušek, K. Engelbrecht, D. Eriksen, S. Dall'Olio, J. Tušek, N. Pryds, A regenerative elastocaloric heat pump, Nat. Energy. 1 (2016) 16134 https://doi.org/10.1038/nenergy.2016.134.
[35] K. Engelbrecht, J. Tušek, D. Eriksen, T. Lei, C.-Y. Lee, J. Tušek, N. Pryds, A regenerative elastocaloric device: experimental results, J. Phys. D. Appl. Phys. 50 (2017) 424006 https://doi.org/10.1088/1361-6463/aa8656.
[36] K. Bartholomé, A. Fitger, A. Mahlke, M. Winkler, O. Schaefer-Welsen, An elastocaloric cooling system based on latent heat transfer, MRS Symp., Boston, MA, 2018 https://www.mrs.org/fall-2018-symposium-sessions/symposium-sessions-detail?code=TP01.
[37] F. Bruederlin, L. Bumke, E. Quandt, M. Kohl, Cascaded SMA-Film Based Elastocaloric Cooling, in: 20th Int. Conf. Solid-State Sensors, Actuators Microsystems Eurosensors XXXIII (TRANSDUCERS EUROSENSORS XXXIII), IEEE, 2019, pp. 1467–1470. https://doi.org/10.1109/TRANSDUCERS.2019.8808605.
[38] R. Snodgrass, D. Erickson, A multistage elastocaloric refrigerator and heat pump with 28 K temperature span, Sci. Rep. 9 (2019) 18532 https://doi.org/10.1038/s41598-019-54411-8.
[39] A. Kitanovski, J. Tušek, U. Tomc, U. Plaznik, M. Ožbolt, A. Poredoš, Magnetocaloric Energy Conversion, Springer, Cham, 2015 https://doi.org/10.1007/978-3-319-08741-2.
[40] M.J. Mahtabi, N. Shamsaei, M.R. Mitchell, Fatigue of Nitinol: The state-of-the-art and ongoing challenges, J. Mech. Behav. Biomed. Mater. 50 (2015) 228–254 https://doi.org/10.1016/j.jmbbm.2015.06.010.
[41] J. Tušek, A. Žerovnik, M. Čebron, M. Brojan, B. Žužek, K. Engelbrecht, A. Cadelli, Elastocaloric effect vs fatigue life: Exploring the durability limits of Ni-Ti plates under pre-strain conditions for elastocaloric cooling, Acta Mater 150 (2018) 295–307 https://doi.org/10.1016/j.actamat.2018.03.032.
[42] H. Hou, J. Cui, S. Qian, D. Catalini, Y. Hwang, R. Radermacher, I. Takeuchi, Overcoming fatigue through compression for advanced elastocaloric cooling, MRS Bull 43 (2018) 285–290 https://doi.org/10.1557/mrs.2018.70.
[43] Y. Wu, E. Ertekin, H. Sehitoglu, Elastocaloric cooling capacity of shape memory alloys – Role of deformation temperatures, mechanical cycling, stress hysteresis and inhomogeneity of transformation, Acta Mater 135 (2017) 158–176 https://doi.org/10.1016/j.actamat.2017.06.012.
[44] J. Chen, K. Zhang, Q. Kan, H. Yin, Q. Sun, Ultra-high fatigue life of NiTi cylinders for compression-based elastocaloric cooling, Appl. Phys. Lett. 115 (2019) 093902 https://doi.org/10.1063/1.5115793.
[45] K. Zhang, G. Kang, Q. Sun, High fatigue life and cooling efficiency of NiTi shape memory alloy under cyclic compression, Scr. Mater. 159 (2019) 62–67 https://doi.org/10.1016/j.scriptamat.2018.09.012.
[46] Z. Tang, D. Li, Quasi-static axial buckling behavior of NiTi thin-walled cylindrical shells, Thin-Walled Struct 51 (2012) 130–138 https://doi.org/10.1016/j.tws.2011.10.007.
[47] D. Jiang, C.M. Landis, S. Kyriakides, Effects of tension/compression asymmetry on the buckling and recovery of NiTi tubes under axial compression, Int. J. Solids Struct. 100–101 (2016) 41–53 https://doi.org/10.1016/j.ijsolstr.2016.07.003.
[48] A.R. Damanpack, M. Bodaghi, W.H. Liao, Snap buckling of NiTi tubes, Int. J. Solids Struct. 146 (2018) 29–42 https://doi.org/10.1016/j.ijsolstr.2018.03.016.
[49] Ž. Ahčin, J. Liang, K. Engelbrecht, J. Tušek, Experimental thermo-hydraulic evaluation of shell-and-tube-like geometries, (n.d.).
[50] J. Tušek, A. Žerovnik, M. Čebron, M. Brojan, S. Zupan, Challenges in designing elastocaloric regenerators, Thermag VIII Int. Conf. Caloric Cool., 2018.
[51] K. Engelbrecht, Future prospects for elastocaloric devices, J, Phys. Energy. 1 (2019) 021001 https://doi.org/10.1088/2515-7655/ab1573.
[52] S. Miyazaki, T. Imai, Y. Igo, K. Otsuka, Effect of cyclic deformation on the pseudoelasticity characteristics of Ti-Ni alloys, Metall. Trans. A. 17 (1986) 115–120 https://doi.org/10.1007/BF02644447.
[53] S. Analysis, Creating Silicon Brains with New Integrated Circuits, Springer, Netherlands, Dordrecht, 2009 https://doi.org/10.1007/978-90-481-2516-6.

[54] S.P. Timoshenko, J.M. Gere, Theory of Elastic Stability (Dover Civil and Mechanical Engineering), Dover Publications (2009) http://www.amazon.com/Theory-Elastic-Stability-Mechanical-Engineering/dp/0486472078.
[55] R.T. Watkins, J.A. Shaw, Unbuckling of superelastic shape memory alloy columns, J, Intell. Mater. Syst. Struct. 29 (2018) 1360–1378 https://doi.org/10.1177/1045389X17733331.
[56] M. Schmidt, J. Ullrich, A. Wieczorek, J. Frenzel, A. Schütze, G. Eggeler, S. Seelecke, Thermal Stabilization of NiTiCuV Shape Memory Alloys: Observations During Elastocaloric Training, Shape Mem. Superelasticity. 1 (2015) 132–141 https://doi.org/10.1007/s40830-015-0021-4.
[57] M. Zhou, Y. Li, C. Zhang, S. Li, E. Wu, W. Li, L. Li, The elastocaloric effect of Ni 50.8 Ti 49.2 shape memory alloys, J, Phys. D. Appl. Phys. 51 (2018) 135303 https://doi.org/10.1088/1361-6463/aaafc2.
[58] K. Engelbrecht, J. Tušek, S. Sanna, D. Eriksen, O.V. Mishin, C.R.H. Bahl, N. Pryds, Effects of surface finish and mechanical training on Ni-Ti sheets for elastocaloric cooling, APL Mater 4 (2016) 064110 https://doi.org/10.1063/1.4955131.
[59] J. Tušek, K. Engelbrecht, L. Mañosa, E. Vives, N. Pryds, Understanding the Thermodynamic Properties of the Elastocaloric Effect Through Experimentation and Modelling, Shape Mem. Superelasticity. 2 (2016) 317–329 https://doi.org/10.1007/s40830-016-0094-8.